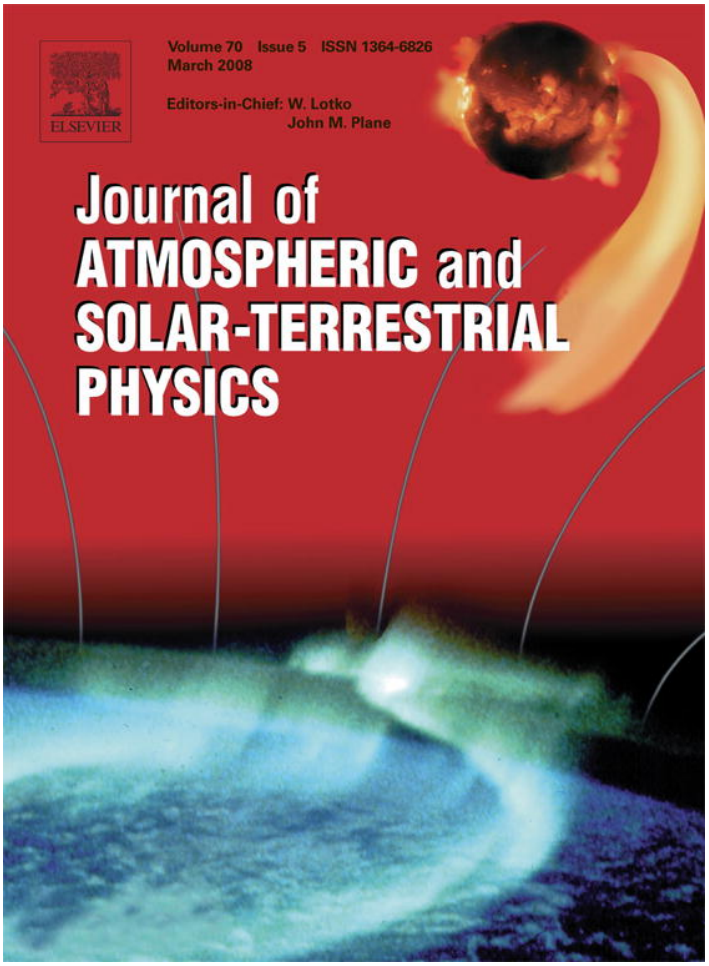

ELSEVIER

Journal of Atmospheric and Solar-Terrestrial Physics 70 (2008) 794–802

Journal of ATMOSPHERIC AND SOLAR-TERRESTRIAL PHYSICS

www.elsevier.com/locate/jastp

The high-latitude thermospheric mass density anomaly: A historical review and a semi-empirical model

Kenneth Moe*, Mildred M. Moe

Space Environment Technologies, 23 Purple Sage, Irvine, CA 92603, USA

Received 12 June 2007; received in revised form 10 October 2007; accepted 27 October 2007
Available online 4 November 2007

Abstract

Recent measurements by the accelerometer on the CHAMP Satellite have confirmed that there are prominent dayside density enhancements at high latitudes at all times. The magnetosphere is the source of the energy which produces these density features. We present a historical review of the observations and a semi-empirical global model which reproduces the observed density increases during geomagnetically quiet times. The parameters in the model were determined over 30 years ago. There is now the opportunity to improve those parameters by using densities measured by the modern accelerometers, as well as by using the latest improvements in describing the UV radiation and the semi-annual density variation. Recent progress in determining physical drag coefficients can enable the model to provide absolute densities.

Keywords: Thermosphere; Magnetosphere; Modeling; Density

1. Historical introduction

When the science of spectroscopy was developed in the 19th and 20th centuries, it was discovered that solar ultraviolet radiation heats, dissociates, and ionizes the upper atmosphere (Mitra, 1947a). Great auroral displays had been observed for millennia, and there were various theories about their cause (Mitra, 1947b). In the 1930s Sydney Chapman and V.C.A. Ferraro were the first to show how streams of ions and electrons emitted from the solar corona could interact with the earth's magnetic field to produce a magnetosphere (Chapman and Ferraro, 1931, 1932). When satellites began flying, Chapman (1960) pointed out that energy from the solar corona continuously flows into the interplanetary gas, and part of this energy flows into the Earth's upper atmosphere at all times. Yet little was known about how solar corpuscular energy entered the Earth's magnetosphere and thermosphere, so the theoretical static diffusion models of Nicolet and Mange (1954) and Nicolet (1960) simply assumed that solar UV radiation was the only energy source for the thermosphere. This idea was carried into the early thermospheric models that fitted satellite drag data to the static diffusion equations. However, Julius Bartels, who was a world authority on geomagnetism, insisted that there was also corpuscular energy flowing into the thermosphere at high latitudes (Jacchia, 1970). As the resolution of satellite drag data improved, Jacchia and Slowey (1963) were able to detect the effects of corpuscular energy that enters the atmosphere during geomagnetic

*Corresponding author. Tel.: +1 949 5091955.
E-mail address: kmmoe@att.net (K. Moe).

1364-6826/$ - see front matter © 2007 Elsevier Ltd. All rights reserved.
doi:10.1016/j.jastp.2007.10.007

storms. Paetzold's model was the first to incorporate a density increase caused by geomagnetic heating (Paetzold, 1962). By 1964, the static diffusion models of Harris and Priester (1964) and Jacchia (1964) also included a geomagnetic storm effect. Jacchia and his assistant, Slowey, introduced the geomagnetic storm effect into Jacchia's static diffusion model by increasing the exospheric temperature as a function of the geomagnetic indices, a_p or k_p (Jacchia and Slowey, 1963; Jacchia, 1964). Nevertheless, the effect of corpuscular energy on the thermospheric density at geomagnetically quiet times was not understood until the Canadians flew their Alouette and ISIS Satellites (Chan and Colin, 1969; Craven, 1970; Heikkila and Winningham, 1971; Shepherd and Thirkettle, 1973; Olson and Moe, 1974; Titheridge, 1976). Thermospheric densities derived from the recent CHAMP/STAR accelerometer data (Luehr et al., 2004; Bruinsma et al., 2004; Liu et al., 2005) confirm the presence of the dayside high-latitude density enhancements which result from energy flowing from the magnetosphere into the thermosphere during geomagnetically quiet times. The location of the density bulge is collocated with the regions of red dayside aurora (Shepherd and Thirkettle, 1973), the locations of electron concentration peaks in the high-latitude ionosphere at geomagnetically quiet times (Chan and Colin, 1969; Titheridge, 1976; Prölss, 2006), and the regions of particle precipitation into the dayside thermosphere from several parts of the magnetosphere (Craven, 1970; Heikkila and Winningham, 1971; Newell and Meng, 1988; Liou et al., 1999). The bulge is centered on the downward projection of the dayside magnetospheric cusp (Olson and Moe, 1974). The wings that extend beyond the region of cusp precipitation were shown by Newell and Meng (1988) to be produced by energetic particles coming around from the plasmasphere and tail.

2. Early evidence from satellite drag

The early evidence for the thermospheric polar density enhancement came in the 1960s, when the US Air Force started launching polar satellites. At first the bulge was inferred from orbital decay data by Jacobs (1967). Later, Ching (1971, 1972) demonstrated that she could improve the correlation between polar satellite drag data and the Jacchia density model by replacing his subsolar density bulge by a high-latitude bulge. In 1967, the Air Force placed an accelerometer on the polar satellite, LOGACS (Bruce, 1973; DeVries, 1972). That experiment defined the bulge more clearly, and confirmed that the high-latitude bulge is larger in magnitude than the subsolar density bulge. Most of the information derived from Air Force polar satellites was unknown to the civilian aeronomic community until Colonel Leonard DeVries (1971) convinced General Samuel Phillips to declassify it in 1971. Because the polar density bulge was unknown to the developers of early static diffusion models that fitted satellite data, the models of Jacchia (1964), Harris and Priester (1964), and Paetzold (1962) did not include such a density bulge at quiet times.

3. Alouette and ISIS

Early in the 1960s, the Canadians began to fly their Alouette Satellites, which carried an ionosonde that looked down on the ionosphere in the Northern Hemisphere. These ionosondes sometimes revealed sudden increases in electron density unlike the patterns seen at lower latitudes. To understand the causative processes, the Canadians then flew the ISIS satellites, which gathered valuable data on topside ionospheric electron concentrations, the aurora, and particle precipitation (Chan and Colin, 1969; Craven, 1970; Heikkila and Winningham, 1971; Shepherd and Thirkettle, 1973). The reports of particle precipitation convinced us that the collaboration of a magnetospheric physicist was essential for understanding thermospheric processes at high latitudes. We asked Willard P. Olson to examine the particle data. He used the ISIS measurements published by Heikkila and Winningham (1971) to outline the region of particle precipitation (Olson, 1972). It is idealized as a lunette-shaped region on the dayside shown as the shaded area in Fig. 1. At the center of the figure is the geographic North Pole. Noon is at the bottom of the figure. The upper dashed circle is the locus of the magnetic pole as the earth rotates. At 23 h UT, the magnetic pole is at the point labeled "23" on the upper circle. To find the center of the lunette arc, we must move 15° equatorward toward the Sun, placing the center of the lunette at point "23" on one of the lower circles which depend on season (winter in Fig. 1).

As the day progresses and the Earth rotates, the center of the lunette arc moves counterclockwise on one of the lower circles. Thus the region shifts

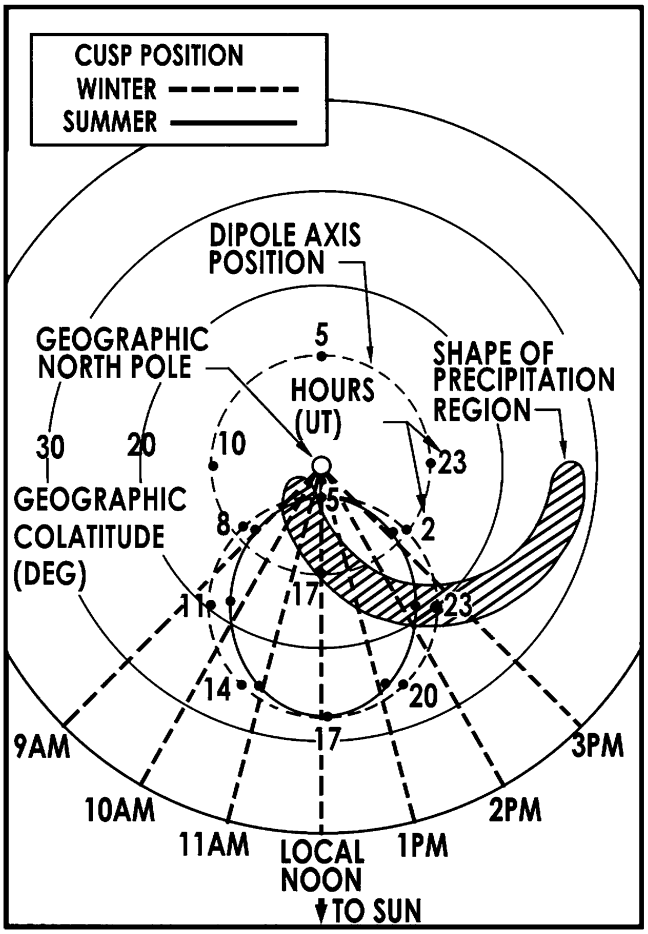

Fig. 1. Willard Olson's model of dayside cusp-related precipitation. As the earth rotates, the shaded precipitation region moves in solar geographic coordinates on one of the lower circles. The central part of the lunette is excited through the cusp. The wings are excited by particles coming around from the plasmasphere and tail.

around in local time and in geographic latitude and longitude. The lunette always faces the sun, with its wings pointing away from the sun. The center of the lunette arc coincides with the footprint of the magnetospheric dayside cusp. This is not to say that all the energy is coming from the cusp. Patrick Newell and his colleagues have discovered that many particles, especially those in the wings of the lunette, are coming from other parts of the magnetosphere, including the plasmasphere and tail (Newell and Meng, 1988; Liou et al., 1999). Moreover, electric fields produce Joule heating in the ionized regions (Cole, 1962, 1966, 1971). Whatever the combination of magnetospheric heating processes, the result is that this energized region is a persistent feature of the high-latitude structure at quiet times.

Measurements of aurora and airglow have become important to density modelers, because the spectroscopic sensors SSUSI and SSULI are being flown on the DMSP Satellites to monitor thermospheric density (Paxton et al., 1998). Spectroscopic measurements can help to improve the density model being used; and density measurements can help to validate and improve the SSUSI and SSULI spectroscopic measurements (Marcos, 2005; Bowman et al., 2007). Fig. 2 shows the contours of red aurora measured during the polar winter by Shepherd and Thirkettle (1973) on ISIS II. Olson's model of the particle precipitation from Fig. 1 is shown shaded for comparison. This comparison confirms that the cusp, plasmasphere, and tail all contribute to energize the lunette-shaped region.

The ionosphere is an integral part of the thermosphere. The upper panel of Fig. 3 shows the topside electron densities measured by the satellite Alouette I on a rare recorded transit of the dayside precipitation region. The lower panel shows the neutral densities measured by the LOGACS accelerometer on pass 31 during May 24, 1967. The satellite crossed the center of the lunette. The densities were normalized to 186 km by Bruce

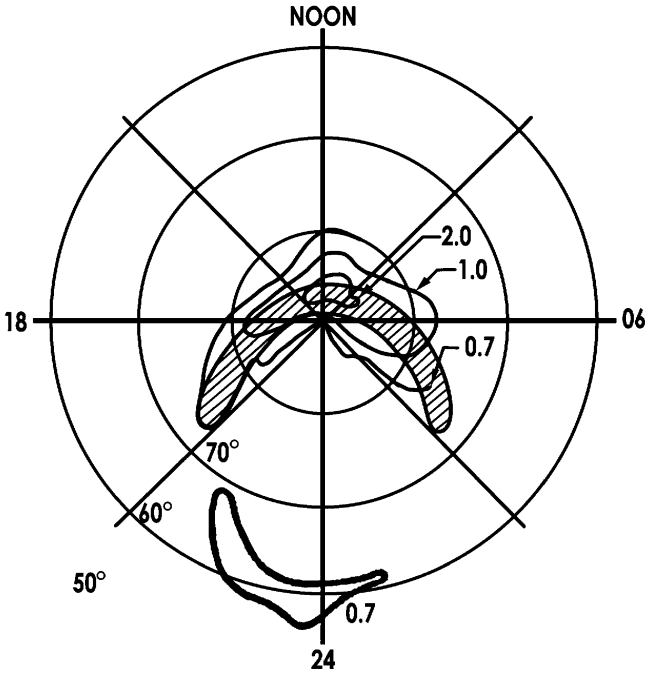

Fig. 2. Red aurora compared with the region of dayside precipitation. Shepherd and Thirkettle's contours of red aurora measured during the polar winter. They resemble the shaded model of the precipitation that excites the quiet dayside aurora. The contour below is a nocturnal aurora caused by precipitation from the tail of the magnetosphere.

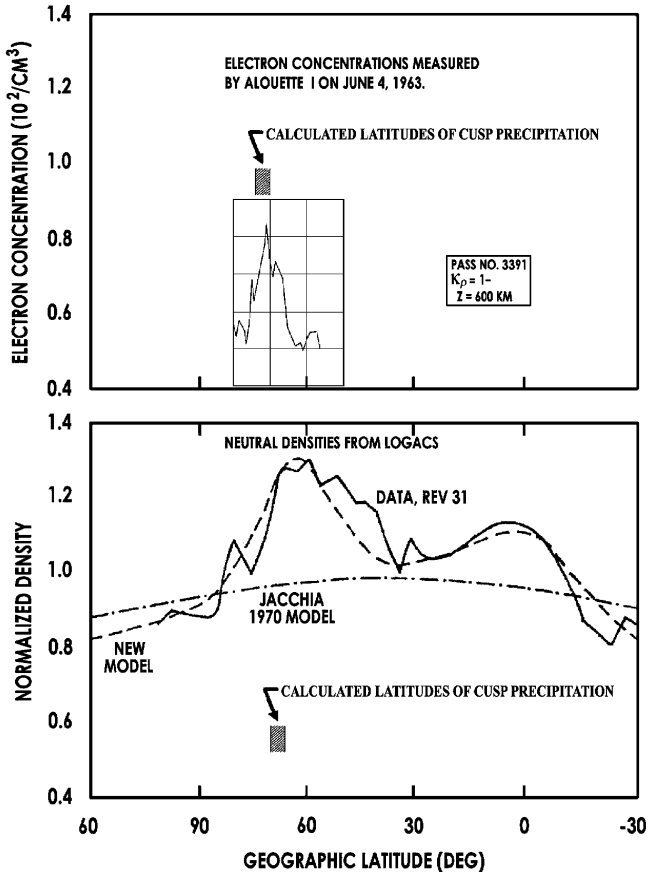

Fig. 3. Cusp-related enhancements of the electron and neutral densities. The upper panel shows the distribution of electron densities measured on Pass 3391 of Alouette 1 as a function of latitude. The lower panel shows the neutral densities measured by LOGACS on orbit 31 as a function of latitude. In both panels, the shaded areas indicate the location of the modeled precipitation region. The neutral densities calculated from Jacchia's model and the present model are also shown.

(1973), using the Jacchia-Bruce density model. The composite figure is shown to demonstrate that the neutral response at times of low geomagnetic activity is spread out more in latitude than the ionospheric response. We believe this spread of the neutral response is caused by the longer time for molecular motions and thermal conduction than the lifetime of electrons. The neutral densities calculated from the Jacchia (1970) model and the present model (described in Section 5.1 below) are also shown for comparison with the LOGACS measurements. This comparison illustrates the importance of including the dayside auroral energy sources in density modeling. All of these measurements and models refer to geomagnetically quiet times.

4. The spades satellite

Fig. 4 shows an example of density measurements made by the SPADES satellite, which carried a spinning pressure (density) gauge (Carter et al., 1969; Moe et al., 1977). The measurements in this figure were made as the satellite passed through the 400 km level in the Southern Hemisphere winter. Since there was no direct UV radiation, the energy was coming mostly through the magnetosphere. The measured density is plotted against geomagnetic colatitude. The density is given as a ratio relative to a static mid-latitude model, the spring/fall model for an exospheric temperature of 1000 K, from the US Standard Atmosphere Supplements, 1966 (ESSA, NASA, and USAF, 1966). The darkened region

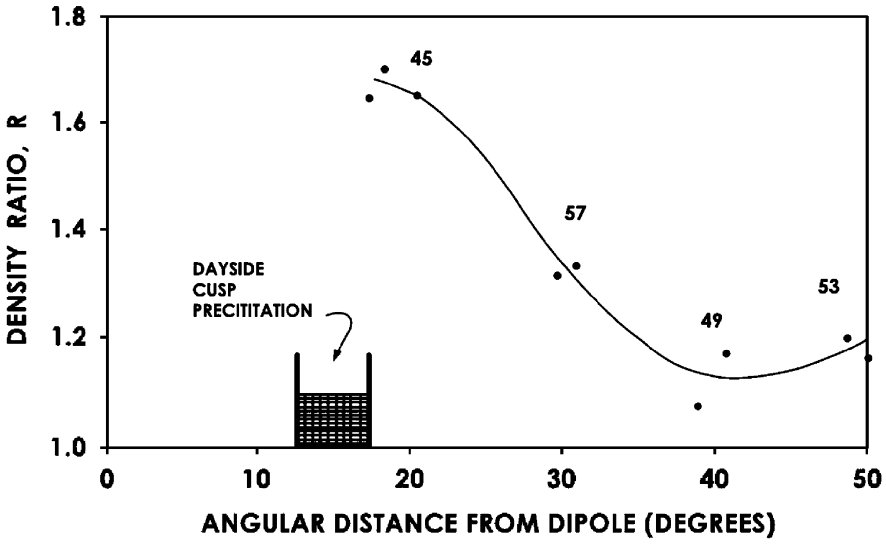

Fig. 4. Densities measured by the SPADES satellite near the southern cusp. Densities measured at quiet times in the Southern Hemisphere also show the influence of the cusp-related energy input.

displaced 15° from the dipole is where the lunette model places the energized region. The numbers 45, 57, etc. refer to the orbital revolution number. The individual points represent densities derived from a single spin period of the pressure gauge. Whereas the energized region related to particle precipitation is narrow, the neutral density response is broad. One might expect this difference, because the times for thermal conduction and mass motions are hours, while the lifetimes even of forbidden excited transitions are seconds.

5. Development of a semi-empirical model including the cusps at geomagnetically quiet times

Based upon the overwhelming evidence from satellite density measurements, electron concentration measurements, red auroral observations, and measurements of particle precipitation through the energized region, a semi-empirical model of the neutral density of the thermosphere was developed (Moe and Moe, 1975; Moe et al., 1975). The neutral density is expressed as a sum of two parts: The first term ρ_u describes the combined effects of the solar ultraviolet heating and various other contributions like the semi-annual variation; the second term $\Delta\rho$ gives the contribution to the density associated with particle precipitation and joule heating coming from magnetospheric sources during times of low geomagnetic activity. The region of density enhancement at high latitudes is associated with the lunette-shaped regions centered on the dayside cusps. Therefore, the model produces a density distribution which depends on universal time as well as on other variables like altitude, latitude, local time, and the solar UV energy source.

5.1. The density function

The mass density ρ is expressed as a function of altitude z, geographic colatitude θ, geographic longitude φ, universal time T, day of the year D, and the measure of the decimetric solar flux F:

$$\rho(z,\theta,\varphi,T,D,F)=\rho_u+\Delta\rho.$$

Here ρ_u is the global density without any contribution from the high-latitude energy sources, whereas the term $\Delta\rho$ represents the density enhancements caused by those sources.

The function

$$\rho_u=\rho_0(z,F)B(z,\theta,t)J(z,\theta,D)Q(z,D),$$

where t is the local time, $t=T+\varphi/15°$. The term ρ_0 (z, F) is an exponential function which gives the height dependence of the mean equatorial density, B (z, θ, t) gives the diurnal variation, J (z, θ, D) gives the latitudinal and seasonal dependence, and Q (z, D) expresses the semi-annual effect.

In the original version, the function ρ_0 (z, F) was chosen to be

$$\rho_0(z,F)=\rho(z_0)\exp[-(z-z_0)/H],$$

where z_0 is the height of the lower boundary of the thermosphere and H is the scale height. A typical value for z_0 was 120 km. The scale height was determined from the expression $H=A(z-103)^{1/2}$ where $A=0.99+0.518\,[(F+F')/110]^{1/2}$.

Here F is the 10 cm solar flux and F' is its average over the preceding 3 months.

The diurnal variation is given by

$$B(z,\theta,t)=[1+(f(t)-1)\sin\theta]^{\mu(z)},$$

where $f(t)$ gives the diurnal variation of density at the equator, and

$$\mu(z)=n[1-\exp\{-(z-z_0)/k\}].$$

Typical values for the parameters are $n=1$ and $k=150$ km.

The function J (z, θ, D) has a more complicated functional form which depends on the colatitude of the sun, the contribution of solar UV heating if all the UV energy were depositied at 200 km altitude, a Fourier series of three terms involving the variables θ and D, and a function introduced to represent energy sources (besides the UV) in the neighborhood of the equator.

The function Q (z, D) has the form

$$Q(z,D)=1+[R(z)-1]G(D),$$

where $R(z)$ is a polynomial in z representing the ratio of the October density maximum to the July minimum. The function G (D) gives the time dependence in a Fourier series of three terms.

The density bulges at high latitudes were constructed by centering them on the locations of the dayside precipitation regions as modeled by Olson (1972). Since the density bulges are wider than the regions of particle precipitation, they have been approximated by a function suggested by observation of atmospheric densities at high latitudes:

$$\Delta\rho=\rho_0(z,F)C(z,\Delta\varepsilon),$$

where $C(z,\Delta\varepsilon)$ is a function of the angular distance $\Delta\varepsilon$ of the point of observation from the central arc of the lunette-shaped precipitation region.

It involves the geomagnetic coordinates of the point of observation, and indirectly the universal time.

Let ε_0 be the angular distance from the central arc of the lunette to the limit of the density bulge. Then when $\Delta\varepsilon \geqslant \varepsilon_0$, $C(z, \Delta\varepsilon) = 0$. However, when $\Delta\varepsilon \leqslant \varepsilon_0$, then

$$C(z) = aL[1 + \cos(\pi\,\Delta\varepsilon/\varepsilon_0)]\{1 - \exp[-(z - z_0)/H]\}.$$

The coefficient "a" is an adjustable parameter of the model, but the value of the coefficient L is determined by the geomagnetic longitude of the point of observation.

The numerical values of the parameters in this semi-empirical model were originally determined over 30 years ago from density data collected by the Bell-MESA accelerometer on the LOGACS satellite and the pressure gauge on the SPADES satellite. As an example of the model output, we show in Fig. 5 a Mercator projection of the global density distribution at an altitude of 400 km at a time of moderate solar activity and low geomagnetic activity. The densities are plotted against geographic east longitude and geographic latitude. At 12 h UT, noon is at zero longitude while the north magnetic pole is eastward at about 290°. The season is approaching northern summer, in late May. Notice that the maximum subsolar density is north of the equator. The high-latitude maximum is about 20% higher than the subsolar maximum. As time progresses, the high-latitude bulge will shift relative to the subsolar bulge. It will shift in geographic latitude as well as in local time. This tells us that we cannot simply use local time and geographic latitude for a complete description of the thermospheric density distribution. We must include the shifting magnetospheric source.

6. Possibilities for improvement

The parameters in the model can now be improved by incorporating recent advances: The description of the semi-annual variation revised by Bowman (2004) can be included in the function Q (z, D); the refinement of solar UV indices by Tobiska (2005) will alter the function ρ_0 (z, F). Schlegel et al. (2005) and Demars and Schunk (2007) have provided more detailed information about the heating in the cusp region, while Newell and his colleagues (Newell and Meng, 1988; Liou et al., 1999) have documented the contributions of the plasmasphere and tail to the dayside auroral heating. Proelss (2006) has shown how the electron density beneath the cusp is affected by geomagnetic disturbance. Faivre et al. (2006) have studied the midnight temperature maximum phenomenon at Arequipa, and Liu et al. (2007) have evaluated the equatorial thermospheric mass density anomaly. All of this new information can improve the representation of the energy sources and physical processes in

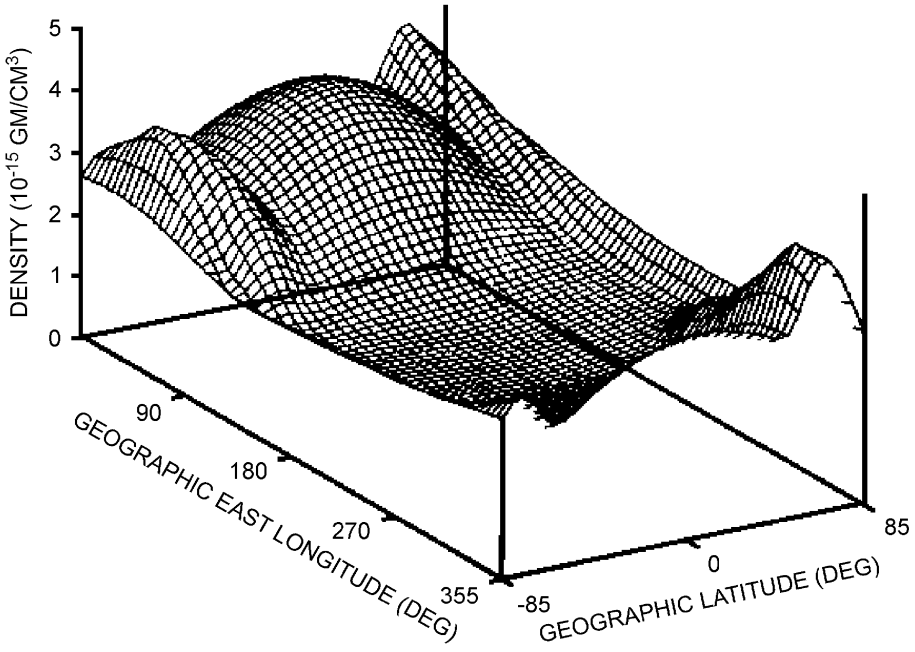

Fig. 5. Global density distribution including dayside auroral energy sources. The polar density bulges at quiet times first reported by Jacobs are clearly visible in this three-dimensional figure.

the model. Furthermore, the large amount of precise density measurements made by the accelerometer on board the CHAMP Satellite (Luehr et al., 2004; Bruinsma et al., 2004; Liu et al., 2005) provides a wealth of data that can eventually improve the parameters that describe the various functions in the model.

The model can be improved in still another way: In the past, the drag coefficients of compactly shaped satellites in free-molecular flow were often assumed to be 2.2 at all altitudes. That assumption has introduced altitude-dependent biases into density measurements, hence into the Jacchia and MSIS density models (Chao et al., 1997; Moe et al., 2004; Moe and Moe, 2005). However, orbital measurements by satellites of various special designs have, in recent years, enabled better drag coefficients to be calculated as a function of altitude for satellites of many shapes (Moe and Moe, 2005; Bowman and Moe, 2005; Moe and Bowman, 2005). This development has made possible the determination of absolute densities from drag data.

Some examples of drag coefficients are shown in Fig. 6. These examples are: A smooth **sphere**; a **flat plate** at normal incidence to the airstream; the spinning **S3-1 Satellite**, which consisted of eight flat plates; and a **short cylinder** terminated by a flat plate that faces the airstream. A **long cylinder** that flies like an arrow would not fit on this graph, because it would have a drag coefficient between 3 and 4, depending mainly on the length-to-diameter ratio and the ambient temperature (Sentman, 1961). The drag coefficients of the long satellites CHAMP and GRACE should also fall in that range (Bowman et al., 2007). In general, the drag coefficients used for those long satellites have been too low. As a consequence, the published densities are too high. Marcos (2005) showed that the densities published for CHAMP are about 37% high, and those published for GRACE about 20% high.

The drag coefficient values shown in Fig. 6 confirm and extend the early work of Sentman. In particular, such improved drag coefficients can be combined with the precise measurements of recent accelerometers to improve the parameters in the empirical model described above. The model would then yield absolute densities at quiet times.

Any density model must eventually treat the case of magnetic storms. The early form of the present model had a version which depended on the value of the geomagnetic planetary amplitude, a_p. However, the storm-time data were not then sufficiently reliable to determine the parameters of the storm-time model with confidence. Bruinsma et al. (2006) have recently used CHAMP and GRACE accelerometer data to study geomagnetic storms. In addition to the bias caused by a low drag coefficient, accelerometer measurements during geomagnetic storms are biased by the great wind system that develops during a storm (Moe and Moe, 1992; Moe et al., 2004). This wind system was first described by Cole (1962, 1966, 1971). It was measured and modeled in two dimensions by Obayashi and Matuura (1971). The storm-time wind system was modeled in great detail in three dimensions by Fuller-Rowell et al. (1994), using a General Circulation Model. Winds greater than1 km/s at high latitudes during storms were first measured by Feess (1973). Such winds can induce errors exceeding 40% in the densities

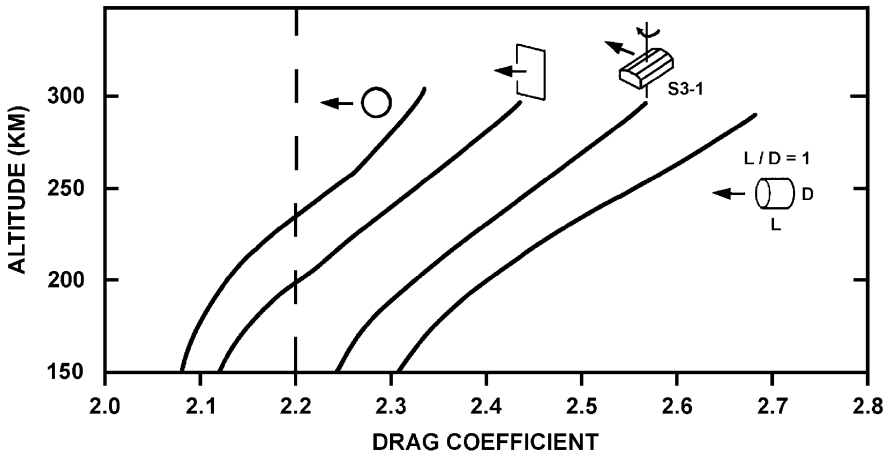

Fig. 6. Drag coefficients of satellites in low-earth orbit. Accurate drag coefficients will enable absolute densities to be measured and modeled at geomagnetically quiet times.

deduced from accelerometers during storms (Moe et al., 2004; Bruinsma et al., 2006). If a mass spectrometer or pressure (density) gauge is flown with the accelerometer, this difficulty can be avoided by simultaneously analyzing the measurements from the accelerometer and the other types of instruments, which interact differently with the airstream. An example of this approach was shown for the case of the satellite, S3-1 (Moe and Moe, 1992; Moe et al., 2004). The present model has the potential to include a version appropriate to geomagnetically disturbed conditions, when accurate storm-time densities become available.

7. Summary

At geomagnetically quiet times there is a large magnetospheric energy source at high latitudes. It produces prominent dayside density enhancements which are dependent on universal time and are in the same locations as ionospheric electron density peaks, the dayside aurora, and particles precipitating from the magnetosphere. The semi-empirical model described here can reproduce this type of neutral density increase, which appears at high latitudes in both hemispheres. Improved orbital data and analyses have recently become available: These can be used to improve the parameters in the model. Recent accelerometer measurements, if combined with improved satellite drag coefficients, can enable the model to provide absolute densities at quiet times.

Acknowledgments

The first version of this model was developed during the period 1972–1975 at the McDonnell Douglas Astronautics Company and the University of California, Irvine, under Contract F44620-72-C-0084 of the Air Force Office of Scientific Research. After the contract ended, further work was performed at the University of California, Irvine. We thank the editor, William Lotko, and the reviewers for many valuable suggestions.

References

Bowman, B.R., 2004. The Semiannual Thermospheric Density Variation From 1970 to 2002 Between 200–1100 km, Paper AAS 04-171. American Astronautical Society Publications Office, San Diego, CA.

Bowman, B.R., Moe, K., 2005. Drag Coefficient Variability at 175–500 km From the Orbit Decay Analysis of Spheres, Paper AAS 05-257. American Astronautical Society Publications Office, San Diego, CA.

Bowman, B.R., Marcos, F.A., Moe, K., Moe, M.M., 2007. Determination of Drag Coefficient Values for CHAMP and GRACE Satellites Using Orbit Drag Analysis, Paper AAS 07-259. American Astronautical Society Publications Office, San Diego, CA.

Bruce, R.W., 1973. Upper Atmospheric Density Determination From LOGACS, in The Low-G Accelerometer Calibration System, vol. II, Report No. TR-0074 (4260-10), vol. II, The Aerospace Corp., El Segundo, CA, pp. 1-1 to 1-43.

Bruinsma, S., Tamagnan, D., Biancale, R., 2004. Atmospheric densities derived from CHAMP/STAR accelerometer observations. Planetary and Space Science 52, 297–312.

Bruinsma, S., Forbes, J.F., Nerem, R.S., Zhang, X., 2006. Thermosphere density response to the 20–21 November solar and geomagnetic storm from CHAMP and GRACE accelerometer data. Journal of Geophysical Research 111, A06303.

Carter, V.L., Ching, B.K., Elliott, D.D., 1969. Atmospheric density above 158 km inferred from magnetron and drag data from the satellite OV1-15 (1968-059A). Journal of Geophysical Research 74, 5083–5091.

Chan, K.L., Colin, L., 1969. Global electron density distributions from topside soundings. Proceedings of the Institute of Electrical and Electronic Engineers 57, 990–1004.

Chao, C.C., Gunning, G.R., Moe, K., Chastain, S.H., Settecerri, T.J., 1997. An evaluation of Jacchia 71 and MSIS 90 atmosphere models with NASA ODERACS decay data. Journal of the Astronautical Sciences 45, 131–141.

Chapman, S., 1960. The Thermosphere—the Earth's Outermost Atmosphere. In: Ratcliffe, J.A. (Ed.), Physics of the Upper Atmosphere. Academic Press, New York and London, pp. 1–16.

Chapman, S., Ferraro, V.C.A., 1931. A new theory of magnetic storms. Terrestrial Magnetism and Atmospheric Electricity 36, 77–98, 171–186.

Chapman, S., Ferraro, V.C.A., 1932. A new theory of magnetic storms (continued). Terrestrial Magnetism and Atmospheric Electricity 37, 147–156, 421–430.

Ching, B.K., 1971. A comparison of drag data with several model atmospheres at altitudes below 200 km. Report TOR 00059 (6110-01)-44, Aerospace Corporation, Los Angeles, CA.

Ching, B.K., 1972. Density variations and atmospheric rotation. In: Bowhill, S.A., Jaffe, L.D., Rycroft, M.A. (Eds.), Space Research XII, vol. 2. Akademie-Verlag, Berlin, pp. 841–846.

Cole, K.D., 1962. Joule heating of the upper atmosphere. Australian Journal of Physics 15, 223–235.

Cole, K.D., 1966. Magnetic storms and associated phenomena. Space Science Reviews 5, 699.

Cole, K.D., 1971. Electrodynamic heating and movement of the thermosphere. Planetary and Space Science 19, 59.

Craven, J.D., 1970. A Survey of electron fluxes. Journal of Geophysical Research 75, 2468–2480.

Demars, H.G., Schunk, R.W., 2007. Thermospheric response to ion heating in the dayside cusp. Journal of Atmospheric and Solar-Terrestrial Physics 69, 649–660.

DeVries, L.L., 1971. Private communication.

DeVries, L.L., 1972. Structure and motion of the thermosphere. In: Bowhill, S.A., Jaffe, L.D., Rycroft, M.A. (Eds.), Space Research XII (GDR).

ESSA, NASA, and USAF, 1966. US Standard Atmosphere Supplements, 1966. Govt. Printing Office, Washington, DC, pp. 39–47.

Faivre, M., Meriwether, J.W., Fesen, C.G., Biondi, M.A., 2006. Climatology of the midnight temperature maximum phenomenon at Arequipa, Peru. Journal of Geophysical Research 111, A06302.

Feess, W.A., 1973. LOGACS wind analysis. In: The Low-G Accelerometer Calibration System, vol. II, Report no. TR-0074(4260-10)-1, vol. II, Aerospace Corp., El Segundo, CA, pp. 7-1 to 7-39.

Fuller-Rowell, T.J., Codrescu, M.V., Moffett, R.J., Quegan, S., 1994. Response of the thermosphere and ionosphere to geomagnetic storms. Journal of Geophysical Research 99, 3893–3914.

Harris, I., Priester, W., 1964. The Upper Atmosphere in the Range from 120 to 800 km. Reprinted in COSPAR International Reference Atmosphere. North-Holland Publishing Co., Amsterdam, 1965.

Heikkila, W.J., Winningham, J.D., 1971. Penetration of magnetosheath plasma to low altitudes through the dayside magnetospheric cusps. Journal of Geophysical Research 76, 883–891.

Jacchia, L.G., 1964. Static diffusion models of the upper atmosphere. Smithsonian Astrophysical Observatory, Special Report no. 170, Cambridge, MA.

Jacchia, L.G., 1970. Private communication.

Jacchia, L.G., Slowey, J., 1963. Atmospheric heating in the auroral zones. Smithsonian Astrophysical Observatory, Special Report no. 136, Cambridge, MA.

Jacobs, R.L., 1967. Atmospheric density derived from the drag of eleven low altitude satellites. Journal of Geophysical Research 72 (5), 1571–1581.

Liou, K., Newell, P.T., Meng, C.-I., Sotirelis, T., Brittnacher, M., Parks, G., 1999. Source region of 1599 MLT auroral bright spots: simultaneous polar UV-images and DMSP particle data. Journal of Geophysical Research 104, A900290.

Liu, H., Luehr, H., Henize, V., Koehler, W., 2005. Global distribution of the thermospheric total mass density derived from CHAMP. Journal of Geophysical Research 110, A04301.

Liu, H., Luehr, H., Watanabe, S., 2007. Climatology of the equatorial thermospheric mass density anomaly. Journal of Geophysical Research 112, A05305.

Luehr, H., Rother, M., Koehler, W., Ritter, P., Grunwaldt, L., 2004. Thermospheric upwelling in the cusp region: evidence from CHAMP observations. Geophysical Research Letters 31, L06805.

Marcos, F.A., 2005. New Measurements of Thermospheric Neutral Density: A Review, Paper AAS 05-251. American Astronautical Society Publications Office, San Diego, CA.

Mitra, S.K., 1947a. The Upper Atmosphere. The Royal Asiatic Society of Bengal, Calcutta, 91–92 and 131–143.

Mitra, S.K., 1947b. The Upper Atmosphere. The Royal Asiatic Society of Bengal, Calcutta, pp. 417–418.

Moe, K., Bowman, B.R., 2005. The Effects of Surface Composition and Treatment on Drag Coefficients of Spherical Satellites, AAS 05-258. AAS Publications Office, San Diego, CA.

Moe, K., Moe, M.M., 1975. A dynamic model of the neutral thermosphere. Report MDC G5891 to AF Office of Scientific Research Under Contract F44620-72-C-0084, McDonnell Douglas Astronautics Co., Huntington Beach, CA.

Moe, K., Moe, M.M., 1992. The deduction of in-track winds from satellite measurements of density and composition. Geophysical Research Letters 19, 1343–1346.

Moe, K., Moe, M.M., 2005. Gas-surface interactions and satellite drag coefficients. Planetary and Space Science 53, 793–801.

Moe, K., Olson, W.P., Moe, M.M., Oelker, G., 1975. A thermospheric model which includes magnetospheric, tropospheric, and ultraviolet energy sources. EOS, Transactions of the American Geophysical Union 56, 626–628.

Moe, K., Moe, M.M., Carter, V.L., Ruggera Jr., M.B., 1977. The correlation of thermospheric densities with charged particle precipitation through the magnetospheric cleft. Journal of Geophysical Research 82, 3304–3306.

Moe, K., Moe, M.M., Rice, C.J., 2004. Simultaneous analysis of multi-instrument satellite measurements of atmospheric density. Journal of Spacecraft and Rockets 41, 849–853.

Newell, P.T., Meng, C.-I., 1988. The cusp and the cleft/boundary layer: low latitude identification and statistical local time variation. Journal of Geophysical Research 93, 14545–14549.

Nicolet, M., 1960. Properties and constitution of the Earth's upper atmosphere. In: Ratcliffe, J.A. (Ed.), Physics of the Upper Atmosphere. Academic Press, New York and London, pp. 17–71.

Nicolet, M., Mange, P., 1954. The dissociation of oxygen in the high atmosphere. Journal of Geophysical Research 59, 15–45.

Obayashi, T., Matuura, N., 1971. Theoretical model of F-region storms. In: Dyer, E.J. (Ed.), Proceedings of the Symposium on Solar-Terrestrial Physics, Washington, DC.

Olson, W.P., 1972. Corpuscular radiation as an upper atmospheric energy source. In: Bowhill, S.A., Jaffe, L.D., Rycroft, M.A. (Eds.), Space Research XII, b. Akademie-Verlag, Berlin, pp. 1007–1013.

Olson, W.P., Moe, K., 1974. Influence of precipitating charged particles on the high-latitude thermosphere. Journal of Atmospheric and Terrestrial Physics 36, 1715–1726.

Paetzold, H.-K., 1962. Model for the variability of the terrestrial atmosphere after satellite acceleration, U. of Cologne. In: Wolverton, R.W. (Ed.), Reprinted in Flight Performance Handbook for Orbital Operations. Wiley, New York and London, 1963, 2-340 to 2-356.

Paxton, L.J., et al., 1998. Interactive interpretation and display of far ultraviolet data. Advances in Space Research 22 (11), 1577–1582.

Proelss, G.W., 2006. Electron temperature enhancement beneath the magnetospheric cusp. Journal of Geophysical Research 111, A07304.

Schlegel, K., Luehr, H., St. Maurice, J.-P., Crowley, G., Hackert, C., 2005. Thermospheric density structures over the polar regions observed with CHAMP. Annales Geophysicae 23, 1659–1672.

Sentman, L.H., 1961. Comparison of the exact and approximate methods for predicting free-molecular aerodynamic coefficients. American Rocket Society Journal 31, 1576–1579.

Shepherd, G.G., Thirkettle, E.W., 1973. Magnetospheric dayside cusp: a topside view of its 6300 A emission. Science 180, 737–739.

Titheridge, J.E., 1976. Ionospheric heating beneath the magnetospheric cleft. Journal of Geophysical Research 81, 3221–3226.

Tobiska, W.K., 2005. Advances in Solar Inputs for Precision Orbit Determination. AAS 05-252. AAS Publications Office, San Diego, CA.